Journal of the Optical Society of America B
OPTICAL PHYSICS

Evaluation of the nonlinear response of plasmonic metasurfaces: Miller's rule, nonlinear effective susceptibility method, and full-wave computation

JÉRÉMY BUTET* AND OLIVIER J. F. MARTIN

Nanophotonics and Metrology Laboratory (NAM), Swiss Federal Institute of Technology Lausanne (EPFL), 1015, Lausanne, Switzerland
**Corresponding author: jeremy.butet@epfl.ch*

Received 1 September 2015; revised 6 November 2015; accepted 7 November 2015; posted 9 November 2015 (Doc. ID 248312); published 8 December 2015

In this article, the second-harmonic generation (SHG) from gold split-ring resonators is investigated using different theoretical methods, namely, Miller's rule, the nonlinear effective susceptibility method, and full-wave computation based on a surface integral equation method. The results confirm that Miller's rule is, in general, not well suited for the description of SHG from plasmonic metasurfaces. On the other hand, the comparison of the nonlinear effective susceptibility method with full-wave computations shows that this method permits us to evaluate second-harmonic (SH) emission patterns from noncentrosymmetric nanoparticles with good accuracy. However, the nonlinear effective susceptibility method fails to reproduce the multipolar nature of the SH emission from centrosymmetric nanoparticles. This shortcoming is attributed to the intrinsic nature of the nonlinear effective susceptibility method, which neglects the exact positions of the nonlinear sources. The numerical implementations of these two methods are also discussed in detail, revealing that the main limitation of the nonlinear effective susceptibility method, aside from the inaccuracy observed in specific cases, is its higher numerical requirements when several emitting directions need to be considered. This limitation stands for most of the numerical methods used for solving Maxwell's equations at the nanoscale. This work provides clear insight into the limitations and advantages of the different methods available for evaluation of SHG from plasmonic metasurfaces. © 2015 Optical Society of America

OCIS codes: (160.3918) Metamaterials; (160.4330) Nonlinear optical materials; (190.2620) Harmonic generation and mixing.

http://dx.doi.org/10.1364/JOSAB.33.0000A8

1. INTRODUCTION

Metasurfaces consist of collections of metamolecules, that is, subwavelength nanostructures such as plasmonic nanoantennas, with unusual electromagnetic properties [1–4]. Metasurfaces are able to control the phase, amplitude, and polarization of light despite their thickness, which is shorter than the wavelength [1–4]. Control of the light properties enables the design of new flat optical components, such as planar lenses [5], Gaussian-to-Bessel beam transformers [6], broadband filters [7], and quarter-wave plates [8], to name a few typical examples of the new possibilities they offer. However, some of the most common optical components, such as optical isolators [9], are based on the nonlinearity of their response; thus, it is important to extend the current understanding of metasurfaces to their nonlinear properties [10]. Optical nonlinearity results in a broad variety of nonlinear processes, ranging from frequency conversion (an electromagnetic wave oscillating at a new, harmonic, frequency is generated from the fundamental wave [11–16]) to the Kerr effect, which results in an intensity-dependent response [17].

In order to design optical components based on the nonlinear response of metasurfaces, the development of analysis methods appropriate for the nonlinear regime is mandatory. In this context, the validity of Miller's rules [18] for the description of nonlinear metasurfaces was recently investigated [19]. Indeed, Miller observed in various piezoelectric crystals that the ratio between the nonlinear susceptibility and the product of the linear susceptibility of the same material at the pump and generated wavelengths is almost constant [18]. This phenomenal rule was subsequently explained using an anharmonic oscillator model [20]. In the framework of plasmonics, several attempts have been made to relate the nonlinear conversion yield of a plasmonic system to its linear far-field properties (scattering or reflectance) at the fundamental and generated wavelengths [Fig. 1(a)]. The anharmonic oscillator model has been successfully applied for the determination of the third-order nonlinear

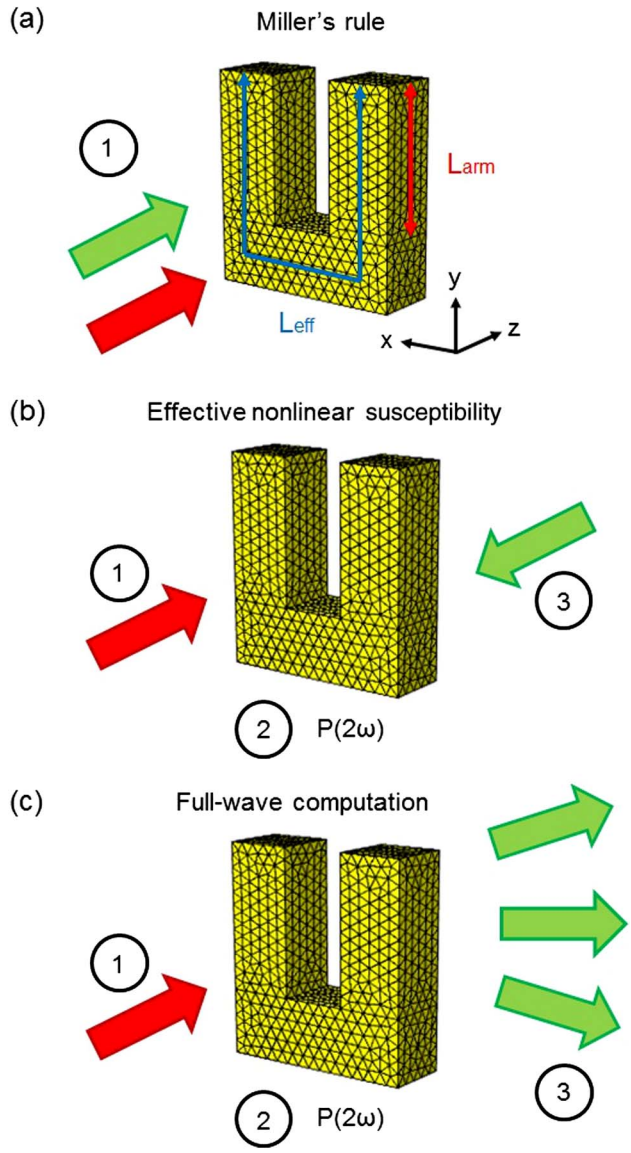

Fig. 1. Different methods used for evaluation of the nonlinear response of plasmonic systems. (a) Miller's rule requires the evaluation of the linear properties at the fundamental and harmonic wavelengths. Plane wave excitations are generally used. (b) Evaluation of the effective nonlinear polarization is composed of three steps: (1) the excitation by the fundamental wave; (2) the computation of the nonlinear polarization; and (3) the evaluation of the overlap integral between the near field driven by a plane wave propagating from the detector and oscillating at the harmonic frequency and the nonlinear polarization. (c) The first two steps for the full-wave computation are the same as in (b), but the last step consists in the direct evaluation of the emission pattern of the nonlinear sources applying the required boundary conditions for the nonlinear electromagnetic wave. The surface mesh is the one used for the SIE simulation reported in this work ($R = 0.30$).

response, i.e., the third-harmonic generation, for plasmonic nanoantennas [21] and metamolecules supporting Fano resonances [22]. In the case of the second-harmonic generation (SHG), Miller's rule is not always fulfilled and seems to stand only for plasmonic nanostructures resonant at the second harmonic (SH) wavelength only, with no resonant behavior at the fundamental wavelength [23,24]. For example, Miller's rule is not able to reproduce either the influence of the metallic split-ring resonators (SRRs) morphology on the SHG [19,25,26] or SH emission pattern from complex coupled plasmonic nanostructures [27]. Although these results seem contradictory at first sight, the differences in the selection rules for second- and third-order nonlinear optical processes explain this discrepancy [28,29]. Indeed, SHG in plasmonic nanostructures involves high-order modes (electric quadrupole [30], electric octupole [31], and magnetic dipole [32], for example), the contributions of which are not considered in Miller's rule because they barely contribute to the linear response. Miller's rule (and the anharmonic oscillator model) has a limited range of application, and other descriptions of the nonlinear response need to be considered.

A linear-nonlinear hybrid method, the so-called nonlinear effective susceptibility method, has thus been proposed as an alternative to Miller's rules in order to bridge the gap between the linear and the second-order nonlinear responses of plasmonic metasurfaces [19,33]. This method is based on Lorentz's reciprocity and attempts to make a direct link between the linear and the nonlinear responses of a scatterer [19]. When far-field properties are considered in Miller's rule, the nonlinear effective susceptibility method attempts to relate the nonlinear conversion yield of a plasmonic system to its linear near-field properties at the fundamental and generated wavelengths. The nonlinear effective susceptibility method exploits the equality between the overlap integral of the field emitted by the nonlinear polarization and a current source located at the detector position and the overlap integral of the field emitted by the current source at the detector position with the nonlinear polarization [33]. This is illustrated in the case of a SRR in Fig. 1(b), where the red and green arrows represent the fundamental excitation and the plane wave propagating from the detector position and oscillating at the SH frequency, respectively. In other words, the evaluation of the nonlinear effective susceptibility involves the computation of the fundamental electric field and the nonlinear surface polarization, and then the evaluation of the overlap integral between the nonlinear surface polarization and the electric field induced by a second incoming plane wave propagating along the SRR-detector axis with a wavelength equal to half the wavelength of the pump wave [Fig. 1(b)]. It worth noting that the nonlinear effective susceptibility method involves the evaluation of the SH surface polarization, the time derivative of which gives the SH currents flowing at the metal surface. This method includes the evaluation of a nonlinear quantity and cannot be considered as a method permitting us to understand the nonlinear properties of metasurfaces directly from the linear ones. It seems fair to classify it as a linear-nonlinear hybrid method. Although the nonlinear effective susceptibility has proved itself to be helpful for the interpretation of experimental results in nonlinear molecular scattering of light [34] and for the description of the nonlinear response of hybrid semiconductor-plasmonic metasurfaces [35], the limitations of this approach for the description of the nonlinear response of pure plasmonic systems have not been discussed in detail so far, although this discussion is important for the future

development of nonlinear plasmonics. Indeed, the evaluation of the effective nonlinear susceptibility can be performed with any numerical method suitable for the computation of the linear response of plasmonic nanoparticles. As a consequence, the implementation of this approach in commercially available electromagnetic solvers (as Comsol Multiphysics, for example) is possible, making it flexible and accessible to researchers who are not experts in numerical methods for solving the Maxwell equations.

In this article, we compare Miller's rule and the nonlinear effective susceptibility method with full-wave computations for the SHG from gold SRRs. All these methods are implemented using a surface integral equation (SIE) formalism [36,37]. The aim is to provide clear insight into which nonlinear properties of metasurfaces can be effectively deduced from these two methods. In particular, we confirm that the nonlinear effective susceptibility method permits us to optimize the SRR geometry for maximal SHG propagating along the incident beam direction [19]. In the present work, we emphasize the suitability of the nonlinear effective susceptibility method and investigate its suitability to reproduce the SHG scattered in different directions.

2. NUMERICAL METHODS

The linear optical responses of the SRRs have been calculated using a surface integral formulation [38]. A plane wave propagating along the z axis is considered in all the computations. The incident wavelength is $\lambda = 1305$ nm. All the nanostructures are considered in a homogeneous refractive index $n = 1.3$, mimicking the presence of a substrate and a 2 nm ITO layer [19]. The dielectric constants for gold are taken from experimental data at the fundamental and SH wavelengths [39].

In Miller's rule, the SH intensity is then given by

$$I_{\mathrm{SHG}} \propto I^2_{x,\mathrm{Scat}}(\omega) I_{y,\mathrm{Scat}}(2\omega), \tag{1}$$

where the subscripts x and y denote an incident wave polarized along the x and y axes, respectively. A plane wave polarized along the y axis is chosen at the SH frequency because SHG polarized along the x axis is forbidden in the forward direction (see below). For the implementation of Miller's rule, the scattered electric field is evaluated 50 μm away from the gold SRRs in the forward direction. Note that the scattered intensity is used here, instead of the total extinction. Indeed, the extinction cross section is the sum of the scattering cross section and of the absorption cross section, meaning that the implementation of Miller's rule based on the extinction at the fundamental and SH frequencies also contains information about the near-field properties.

In the nonlinear effective susceptibility method, the SH electric field is given by the following surface integral [19]:

$$\mathbf{E}_{\mathrm{SHG}} \propto \iint \chi_{\mathrm{surf},nnn} E^2_n(\omega) E_n(2\omega) \mathrm{d}S, \tag{2}$$

where the integration is performed over the SRR surface. For the sake of simplicity, only the component $\chi_{\mathrm{surf},nnn}$ of the surface tensor is considered, where n denotes the component normal to the surface. Indeed, recent experimental results indicate that this term dominates the surface response of metallic nanoparticles [40,41]. The electric fields considered correspond to the near field for the excitation by the fundamental wave ($E^2_n(\omega)$) and the near field driven by a plane wave propagating from the detector ($E_n(2\omega)$). The electric near-field is evaluated 1 nm away from the metal surface. The SH intensity is obtained by multiplying $\mathbf{E}_{\mathrm{SHG}}$ by its complex conjugate.

For the full-wave computations of SHG, the magnetic and electric linear surface currents are used for the evaluation of the fundamental electric fields just below the gold surfaces and then utilized for the calculation of the surface SH polarization [36,37]. The SH surface currents are obtained solving the SIE formulation, taking into account the nonlinear polarization and enforcing the boundary conditions at the nanostructure surfaces [42]. With this method, the SH electric field can be accurately evaluated in the near- and far-field regions (Fig. 2). All these methods have been implemented in the undepleted pump approximation. The relative computation time for the effective nonlinear susceptibility method using SIE to compute the linear response at the fundamental and SH wavelengths and complete computation of the SHG with

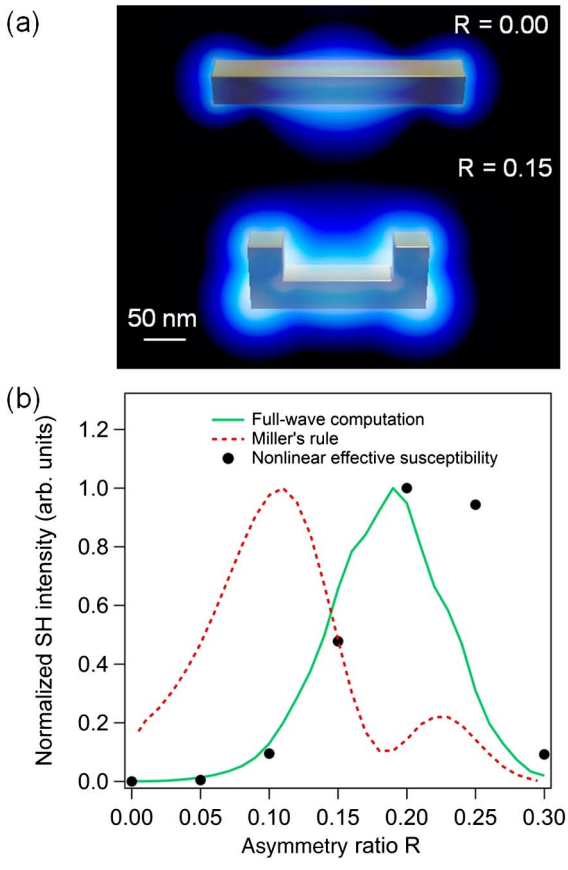

Fig. 2. (a) SH near-field close to two split-ring resonators with asymmetry ratio $R = 0$ (top) and $R = 0.15$ (bottom). The asymmetry ratio R is defined as the ratio between the length of the side arms L_{arm} and the effective length L_{eff}. (b) SH intensity from SRRs with asymmetry ratio R ranging from 0 to 0.30 evaluated using Miller's rule, the nonlinear effective susceptibility, and full-wave computations based on SIE. See the main text for details on the implementation of each method.

SIE becomes an important issue for researchers. Note that the evaluation of the effective nonlinear susceptibility with other numerical methods based on volume discretization, such as the finite element method, for example, is even more time-consuming.

For both methods, the first step is the evaluation of the linear response at the fundamental frequency. The surface mesh used for describing the SRRs studied in this work are composed of approximately 2100 triangles and 3300 edges, resulting in a $N \times N$ linear SIE matrix with $N = 6600$. The resolution of the linear equation system with LU decomposition requires approximately 1.5 N^3 operations. In the effective nonlinear susceptibility evaluation, a second linear computation, involving the plane wave coming from the detector and oscillating at the SH frequency, must be performed and needs the same number of operations. Note that, in the SIE formalism, the LU decomposition needs to be done only one time for a given frequency, whatever the number of excitation conditions [37]. This is benefic for the evaluation of the effective nonlinear susceptibility, for which it is necessary to consider a new excitation (at the SH wavelength) for each position of the detector. In the complete computation of SHG with SIE, the matrix is slightly larger ($N = 9900$ in this case) due to the specific formulation resulting from the boundary conditions, taking into account the nonlinear surface polarization [35,36]. This means that the resolution of the new linear system of equations requires three times more operation than for the linear response. The full-wave method permits us to evaluate the SH field at any point of space without the solution for any additional system of equations [36,37]. As a consequence, the effective nonlinear susceptibility method using SIE to compute the linear response is two times faster than the complete computation of the SHG with SIE.

Note that the lower computation time of the former method is due to the specificity of SIE, which avoids the LU decomposition for each excitation condition. If we neglect this possibility, as is the case for other standard numerical methods in plasmonics, but still consider that the time computation is limited by the LU decomposition, the full-wave computation of SHG would be more efficient than the effective nonlinear susceptibility method for more than three experimental configurations. Furthermore, to generate the results plotted in one panel of Fig. 3 with 1 deg accuracy, the effective nonlinear susceptibility method would be approximately 200 times more time-consuming than the full-wave SIE method.

3. RESULTS AND DISCUSSION

The SRRs considered in this work are defined by two important geometry parameters (see Fig. 1). The first important parameter is the effective length L_{eff} corresponding to the total length of the SRR. The length L_{eff} is fixed to 300 nm, and all the SRRs have the same volume and surface area. The second important parameter is the asymmetry ratio R, which is defined as the ratio between the length of the side arms L_{arm} and the effective length L_{eff}. For example, SRRs with asymmetry ratio $R = 0$ and 0.15 are shown in Fig. 2. All of the SRRs have a 40 nm × 40 nm section. The SHG from SRRs with asymmetry ratios R ranging from 0 to 0.30 has been evaluated in the far field, 50 μm away from the plasmonic nanostructures, on the z axis in the forward direction using full-wave computations [see Fig. 2(b)]. The obtained dependence is in good agreement with the experimental results reported in [19]: the maximum SHG is obtained for an asymmetry ratio R slightly smaller than $R = 0.20$, as experimentally observed {see Fig. 2(c) in Ref. [19]}. This first result confirms that full-wave SIE is able to accurately compute the SHG from plasmonic nanostructures. Now, we compare these results to the prediction of Miller's rule and of the nonlinear effective susceptibility based

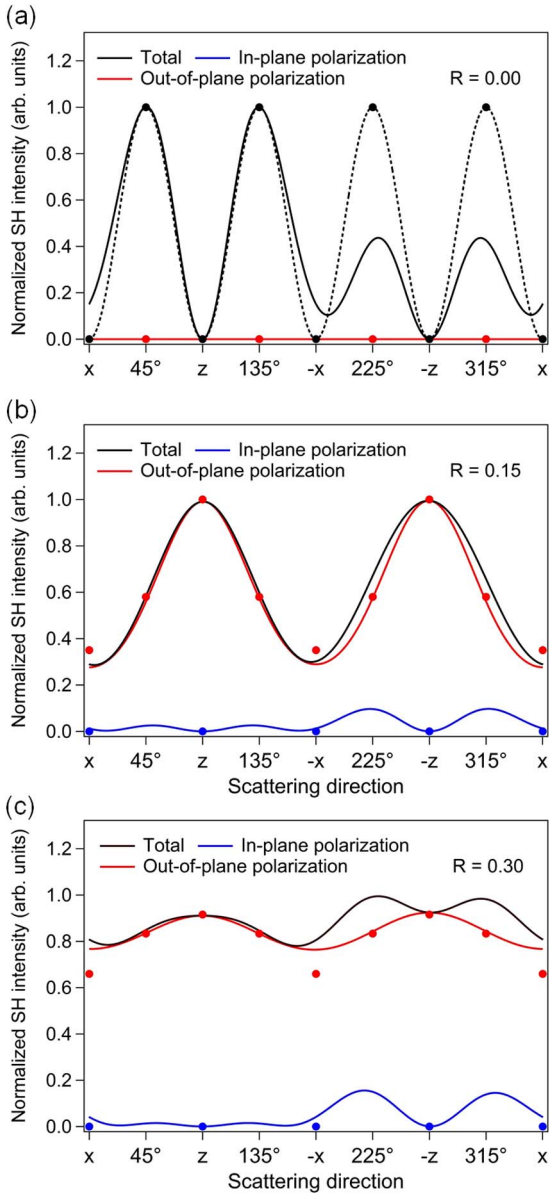

Fig. 3. Far-field SH intensity scattered in the (O, x, z) plane as a function of the scattering angle for split-ring resonators with asymmetry ratios (a) $R = 0.00$, (b) $R = 0.15$, and (c) $R = 0.30$ evaluated using the full-wave method (full lines) and the nonlinear effective susceptibility method (dots). The total SH intensity is shown in black and the contributions of the SH waves polarized into and perpendicular to this plane are shown in blue and red, respectively. In panel (a), the dashed line shows a pure quadrupolar emission.

on an SIE electromagnetic solver. As reported in [19], Miller's rule is not able to predict the optimal SRR geometry. Indeed, Miller's rule indicates that the SHG is maximal for an asymmetry ratio $R = 0.10$, far from the experimental observations [19] and the value obtained with full-wave computations. Contrary to Miller's rule, the nonlinear effective susceptibility method is able to determine the asymmetry ratio resulting in the highest SH intensity ($R \sim 0.20$). However, the use of the nonlinear effective susceptibility method for the determination of the SH emission pattern has not been discussed so far.

To do so, the SH emission patterns have been first computed using full-wave computations. Figure 3 shows the SH intensity as a function of the scattering angle in the (O, x, z) plane for three different gold SRRs. The asymmetry ratio R ranges from 0.00 to 0.30. For the smallest asymmetry ratio, the SH wave polarized perpendicular to the scattering plane (along the y axis) vanishes for any scattering angle. This behavior is due to the nanostructure symmetry. Indeed, the SH sources standing on the top and bottom surfaces of the nanorods perfectly cancel each other in this configuration. On the contrary, the SH wave polarized into the scattering plane is maximal at +45° and +135°. Indeed, for $R = 0.00$, the gold nanostructure corresponds to a straight bar with a length $L = 300$ nm and is therefore centrosymmetric. In this case, the SH electric field must be contained in the symmetry plane, i.e., the (O, x, z) plane in this case. For an incident wave polarized along the x axis, the SH intensity must vanish in the forward and backward directions [43,44], irrespective of the polarization of the SH wave, and the SH intensity is maximal in an arbitrary scattering direction, which depends on the nanostructure properties at the fundamental and SH wavelengths (see Figs. 4–7). It is also interesting to note that the SH intensity at +45° and +135° differs from that at 225° and 315°. The same behavior has been experimentally observed in angle-resolved SH scattering patterns from centrosymmetric silver nanospheres [45]. For SRRs with higher asymmetry ratio ($R = 0.15$ or 0.30), the SH wave is mainly polarized perpendicular to the (O, x, z) plane. This is due to the noncentrosymmetric shapes of these SRRs [see Fig. 2]. Due to the (O, x, z) symmetry plane for the SH field, the description of the SH wave must involve even modes, in the sense of the parity and relative to the (O, x, z) plane, corresponding to two dipoles pointing along the y axis and supported by each SRR arm, producing a strong SH signal [46,47]. These results demonstrate that the polarization of the SH wave depends on the nanoparticle geometry and that its polarization varies with the scattering angle.

In general, the direction of the maximal SH intensity results from the interference between multipoles. Indeed, as mentioned in the introduction, SHG from centrosymmetric nano-objects is forbidden in the electric dipole approximation, and the inclusion of higher multipoles is, in general, required to accurately describe it. The transition from a dipolar SH emission from small plasmonic nanospheres induced by shape effects to a quadrupolar SH emission induced by retardation is a good example of the link between the geometry of the nanostructure and the properties of the electromagnetic fields at the fundamental and SH frequencies [48,49]. In order to determine its ability to probe the multipolar nature of the SH emission from gold SRRs resulting from shape and retardation effects, the nonlinear effective susceptibility method was applied considering "probing" plane waves with various angles and polarization states. The case of the noncentrosymmetric SRRs ($R = 0.15$ and $R = 0.30$) is discussed first [see Figs. 3(b) and 3(c)]. For example, plane waves with incident angles of 45°, 135°, 225°, and 315° and z polarization impinging on gold SRRs with asymmetry ratios $R = 0.15$ and $R = 0.30$ have been considered. The results are independent of the propagation directions, as expected from symmetry considerations and confirming the validity of our numerical implementation of the nonlinear effective susceptibility method. The ratio between the SH intensity at these scattering angles and that in the forward direction is 0.54 for $R = 0.15$ and 0.86 for $R = 0.30$. These values are in very good agreement with the full-wave computations (0.58 for $R = 0.15$ and 0.91 for $R = 0.30$), confirming that the nonlinear effective

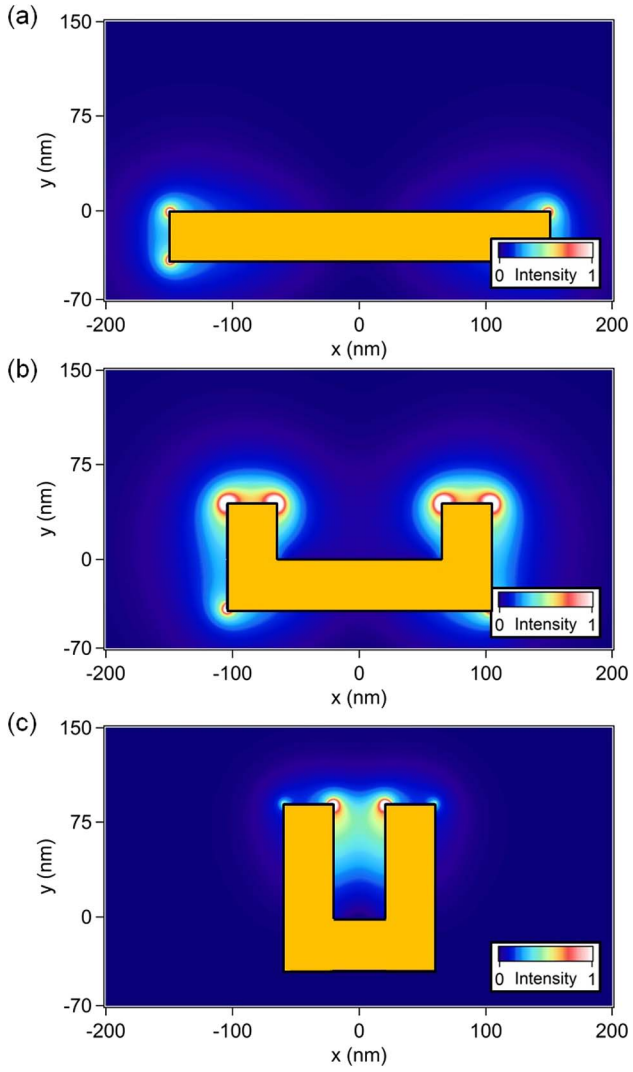

Fig. 4. Fundamental near-field intensity in the vicinity of split ring resonator with asymmetry ratios (a) $R = 0$, (b) $R = 0.15$, and (c) $R = 0.30$. The incident wavelength is $\lambda = 1305$ nm.

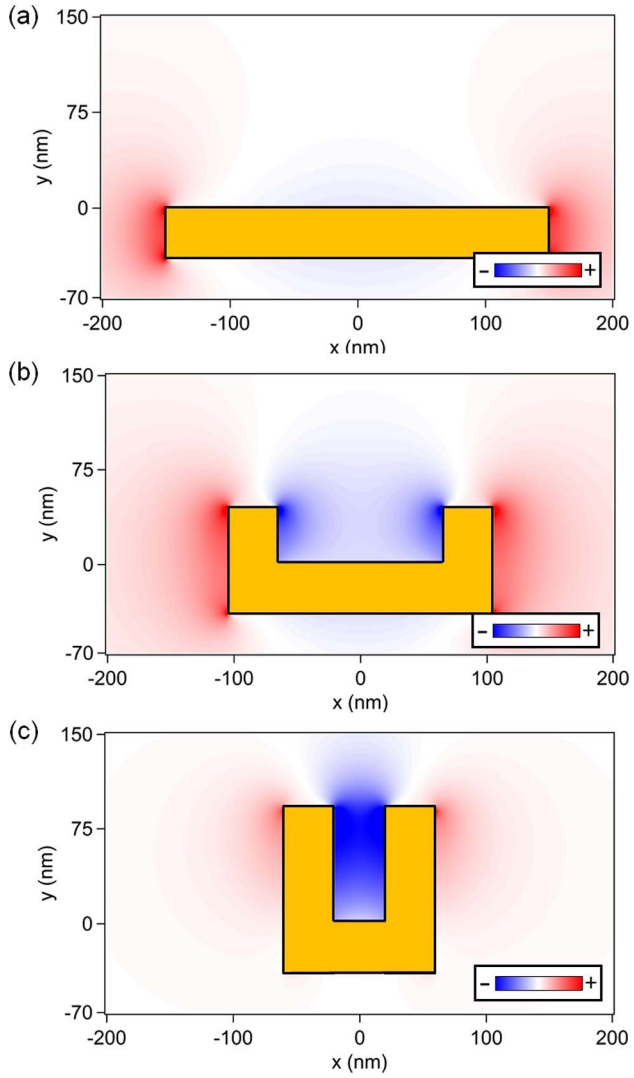

Fig. 5. Real part of the x component of the fundamental field in the vicinity of split ring resonator with asymmetry ratios (a) $R = 0$, (b) $R = 0.15$, and (c) $R = 0.30$. The incident wavelength is $\lambda = 1305$ nm.

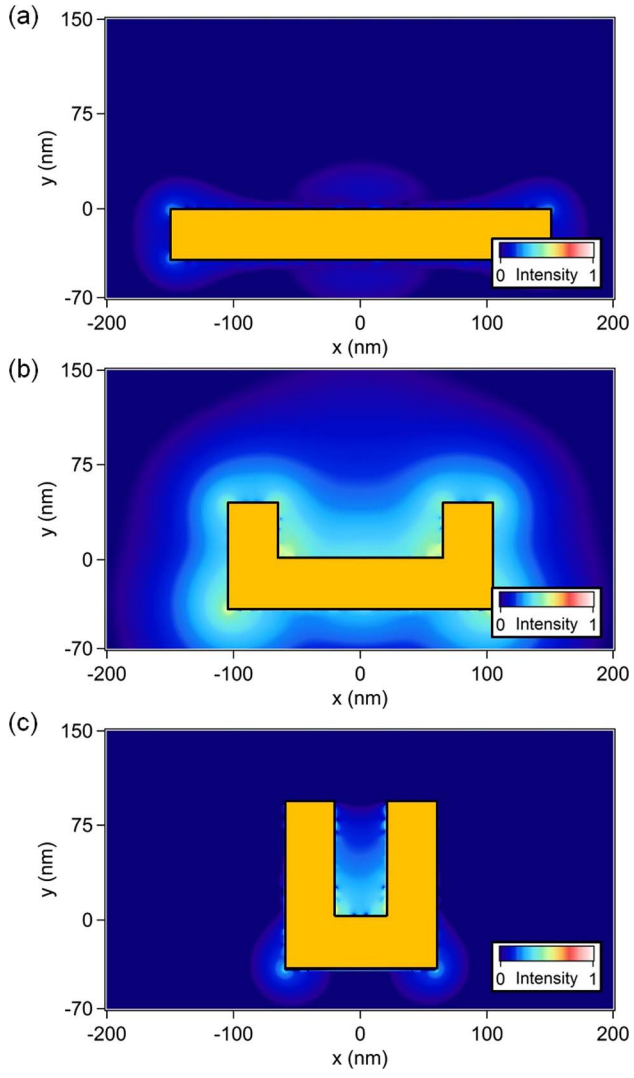

Fig. 6. SH near-field intensity in the vicinity of split ring resonator with asymmetry ratios (a) $R = 0$, (b) $R = 0.15$, and (c) $R = 0.30$. The fundamental wavelength is $\lambda = 1305$ nm.

susceptibility method is able to reproduce with good accuracy the SH emission resulting from shape effects. Now, we turn our attention to centrosymmetric nanoparticles, the SRR for which the asymmetry ratio vanishes (i.e., a gold nanorod). In this case, the effective nonlinear susceptibility methods predict that the SH intensities scattered at 45°, 135°, 225°, and 315° are identical. This is not the case for the full-wave computations, which reveal a stronger SH intensity at 45° and 135°. This discrepancy can be explained as follows: It is now established that the parity of the SH modes differs, in general, from that of the fundamental modes [28,29,50,51]. The parity of the mode is conveniently revealed by the real part of the x component of the electric field as previously used: For the fundamental field driven by an incoming plane wave propagating along the z axis, the (O, x, z) plane is an antisymmetry plane, and the excited mode is odd (see Fig. 5). In contrast, the (O, x, z) plane is a symmetry plane for the SH electromagnetic fields and the excited SH mode is even (see Fig. 7). However, the use of "probing" plane waves with oblique incidence breaks the symmetry such that even and odd modes are simultaneously excited [52]. The modes involved in the description of the SH wave are then filtered through Eq. (2). The discrepancy between the predictions of the nonlinear effective susceptibility method and those of full-wave computations may be related to the fact that the positions of the nonlinear sources are not considered in the nonlinear effective susceptibility method. This approximation modifies the relative weights of the different multipolar moments in the nonlinear response and the SH emission patterns resulting from the interferences between multipoles [31]. These results demonstrate that the nonlinear effective susceptibility method is not an efficient method in the case of centrosymmetric plasmonic metamolecules. Furthermore, the link between the linear and the nonlinear responses is not straightforward because the multipolar nature of the scattered field is weakly expressed in the linear regime.

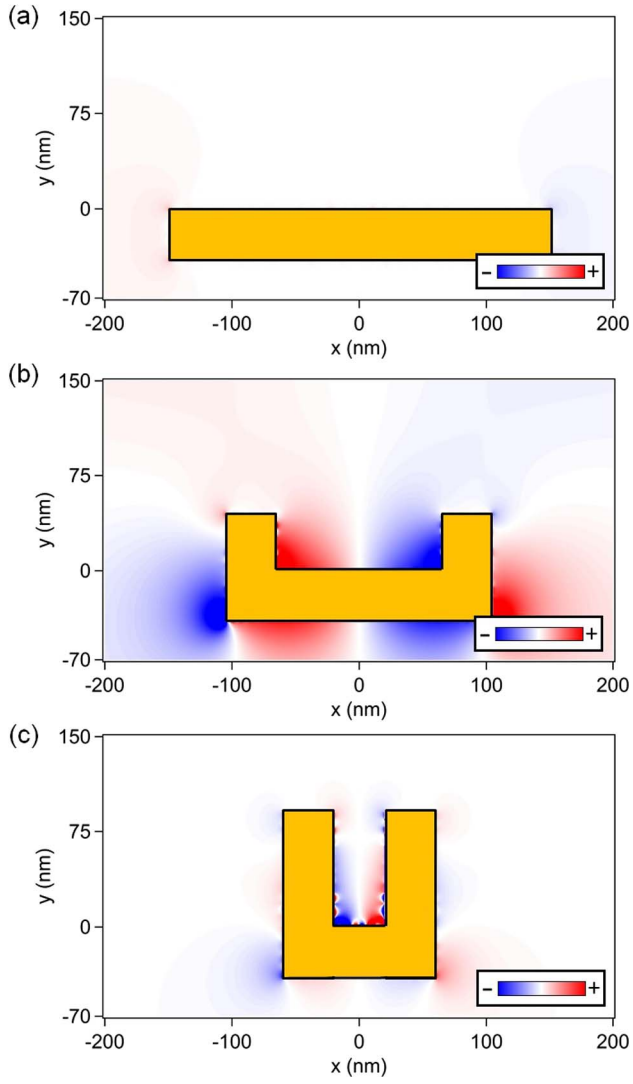

Fig. 7. Real part of the x component of the SH field in the vicinity of split ring resonator with asymmetry ratios (a) $R = 0$, (b) $R = 0.15$, and (c) $R = 0.30$. The incident wavelength is $\lambda = 1305$ nm.

4. CONCLUSION

In conclusion, we have performed a comparison based on an SIE formalism between full-wave computations, Miller's rule, and the nonlinear effective susceptibility method for the description of the SHG from gold SRRs. First, this comparison confirms that Miller's rule is not able to determine the optimal geometry resulting in the highest SH signal [19]. The corresponding discrepancy can be quite important, meaning that this rule cannot be blindly applied for arbitrary plasmonic systems, despite its successful utilizations for specific cases [23,24]. On the other hand, the comparison between the predictions from full-wave computations and those from the nonlinear effective susceptibility method reveals good agreement for noncentrosymmetric metallic nanoparticles. Indeed, this comparison shows, for the first time, that the nonlinear effective susceptibility method is able to reproduce the SH emissions from noncentrosymmetric gold SRRs with good accuracy. However, this method fails to reproduce the multipolar nature of the SH emission from centrosymmetric nanoparticles, induced by retardation effects. The nonlinear effective susceptibility method is thus a plausible alternative to full-wave computations, which are difficult to implement for researchers not involved in the numerical modeling of nanosystems; it must, however, be used with care, as demonstrated in this work. Due to its simple implementation, which is possible in commercially available solvers, the nonlinear effective susceptibility will undoubtedly be part of future developments of nonlinear plasmonic metamolecules with noncentrosymmetric shapes.

Funding. Swiss National Science Foundation (SNSF) (200020_153662).

REFERENCES

1. A. V. Kildishev, A. Boltasseva, and V. M. Shalaev, "Planar photonics with metasurfaces," Science **339**, 1232009 (2013).
2. N. Yu and F. Capasso, "Flat optics with designer metasurfaces," Nat. Mater. **13**, 139–150 (2014).
3. M. Kim, A. M. H. Wong, and G. V. Eleftheriades, "Optical Huygens' metasurfaces with independent control of the magnitude and phase of the local reflection coefficients," Phys. Rev. X **4**, 041042 (2014).
4. N. Meinzer, W. L. Barnes, and I. R. Hooper, "Plasmonic meta-atoms and metasurfaces," Nat. Photonics **8**, 889–898 (2014).
5. F. Aieta, P. Genevet, M. A. Kats, N. Yu, R. Blanchard, Z. Gaburro, and F. Capasso, "Aberration-free ultrathin flat lenses and axicons at telecom wavelengths based on plasmonic metasurfaces," Nano Lett. **12**, 4932–4936 (2012).
6. C. Pfeiffer and A. Grbic, "Metamaterials Huygen's surfaces: tailoring wave fronts with reflectionless sheets," Phys. Rev. Lett. **110**, 197401 (2013).
7. Z. H. Jiang, S. Yun, L. Lin, J. A. Bossard, D. H. Werner, and T. S. Mayer, "Tailoring dispersion for broadband low-loss optical metamaterials using deep-subwavelength inclusions," Sci. Rep. **3**, 1571–1579 (2013).
8. N. Yu, F. Aieta, P. Genevet, M. A. Kats, Z. Gaburro, and F. Capasso, "A broadband, background-free quarter-wave plate based on plasmonic metasurfaces," Nano Lett. **12**, 6328–6333 (2012).
9. Y. Shi, Z. Yu, and S. Fan, "Limitation of nonlinear optical isolators due to dynamic reciprocity," Nat. Photonics **9**, 388–392 (2015).
10. A. E. Minovich, A. E. Miroshnichenko, A. Y. Bykov, T. V. Murzina, D. N. Neshev, and Y. S. Kivshar, "Functional and nonlinear optical metasurfaces," Laser Photon. Rev. **9**, 195–213 (2015).
11. H. Husu, R. Siikanen, J. Mäkitalo, J. Lehtolahti, J. Laukkanen, M. Kuittinen, and M. Kauranen, "Metamaterials with tailored nonlinear optical response," Nano Lett. **12**, 673–677 (2012).
12. R. Czaplicki, H. Husu, R. Siikanen, J. Mäkitalo, and M. Kauranen, "Enhancement of second-harmonic generation from metal nanoparticles by passive elements," Phys. Rev. Lett. **110**, 093902 (2013).
13. E. A. Mamonov, I. A. Kolmychek, S. Vandendriessche, M. Hojeij, Y. Ekinci, V. K. Valev, T. Verbiest, and T. V. Murzina, "Anisotropy versus circular dichroism in second harmonic generation from fourfold symmetric arrays of G-shaped nanostructures," Phys. Rev. B **89**, 121113(R) (2014).
14. H. Suchowski, K. O'Brien, Z. J. Wong, A. Salandrino, X. Yin, and X. Zhang, "Phase mismatch-free nonlinear propagation in optical zero-index materials," Science **342**, 1223–1226 (2013).
15. G. Li, S. Chen, N. Pholchai, B. Reineke, P. W. H. Wong, E. Y. B. Pun, K. W. Cheah, T. Zentgraf, and S. Zhang, "Continuous control of the nonlinearity phase for harmonic generations," Nat. Mater. **14**, 607–612 (2015).
16. N. Segal, S. Keren-Zur, N. Hendler, and T. Ellenbogen, "Controlling light with metamaterials-based nonlinear photonic crystals," Nat. Photonics **9**, 180–184 (2015).
17. H. Baida, D. Mongin, D. Christofilos, G. Bachelier, A. Crut, P. Maioli, N. Del Fatti, and F. Vallée, "Ultrafast nonlinear optical response of a

single gold nanorod near its surface plasmon resonance," Phys. Rev. Lett. **107**, 057402 (2011).
18. R. C. Miller, "Optical second harmonic generation in piezoelectric crystal," Appl. Phys. Lett. **5**, 17–19 (1964).
19. K. O'Brien, H. Suchowski, J. Rho, A. Salandrino, K. Boubacar, X. Yin, and X. Zhang, "Predicting nonlinear properties of metamaterials from the linear response," Nat. Mater. **14**, 379–383 (2015).
20. C. Garrett and F. Robinson, "Miller's phenomenological rule for computing nonlinear susceptibilities," IEEE J. Quantum Electron. **2**, 328–329 (1966).
21. M. Hentschel, T. Utikal, H. Giessen, and M. Lippitz, "Quantitative modeling of the third harmonic emission spectrum of plasmonic nanoantennas," Nano Lett. **12**, 3778–3782 (2012).
22. B. Metzger, T. Schumacher, M. Hentschel, M. Lippitz, and H. Giessen, "Third harmonic generation in complex plasmonic Fano structures," ACS Photon. **1**, 471–476 (2014).
23. B. Metzger, L. Gui, J. Fuchs, D. Floess, M. Hentschel, and H. Giessen, "Strong enhancement of second harmonic emission by plasmonic resonances at the second harmonic wavelength," Nano Lett. **15**, 3917–3922 (2015).
24. H. Linnenbank and S. Linden, "Second harmonic generation spectroscopy on second harmonic resonant plasmonic metamaterials," Optica **2**, 698–701 (2015).
25. M. W. Klein, C. Enkrich, M. Wegener, and S. Linden, "Second-harmonic generation from magnetic metamaterials," Science **313**, 502–504 (2006).
26. S. Linden, F. B. P. Niesler, J. Förstner, Y. Grynko, T. Meier, and M. Wegener, "Collective effects in second-harmonic generation from split-ring-resonator arrays," Phys. Rev. Lett. **109**, 015502 (2012).
27. J. Butet and O. J. F. Martin, "Fano resonances in the nonlinear optical response of coupled plasmonic nanostructures," Opt. Express **22**, 29693–29707 (2014).
28. M. Finazzi, P. Biagioni, M. Celebrano, and L. Duò, "Selection rules for second-harmonic generation in nanoparticles," Phys. Rev. B **76**, 125414 (2007).
29. J. Butet, S. Dutta-Gupta, and O. J. F. Martin, "Surface second-harmonic generation from coupled spherical plasmonic nanoparticles: eigenmode analysis and symmetry properties," Phys. Rev. B **89**, 245449 (2014).
30. J. Butet, J. Duboisset, G. Bachelier, I. Russier-Antoine, E. Benichou, C. Jonin, and P.-F. Brevet, "Optical second harmonic generation of single metallic nanoparticles embedded in a homogeneous medium," Nano Lett. **10**, 1717–1721 (2010).
31. J. Butet, G. Bachelier, I. Russier-Antoine, C. Jonin, E. Benichou, and P.-F. Brevet, "Interference between selected dipoles and octupoles in the optical second-harmonic generation from spherical gold nanoparticles," Phys. Rev. Lett. **105**, 077401 (2010).
32. S. Kruk, M. Weismann, A. Y. Bykov, E. A. Mamonov, I. A. Kolmychek, T. Murzina, N. C. Panoiu, D. N. Neshev, and Y. S. Kivshar, "Enhanced magnetic second-harmonic generation from resonant metasurfaces," ACS Photonics **2**, 1007–1012 (2015).
33. S. Roke, M. Bonn, and A. V. Petukhov, "Nonlinear optical scattering: the concept of effective susceptibility," Phys. Rev. B **70**, 115106 (2004).
34. S. Roke and G. Gonella, "Nonlinear light scattering and spectroscopy of particles and droplets in liquids," Ann. Rev. Phys. Chem. **63**, 353–378 (2012).
35. J. Lee, M. Tymchenko, C. Argyropoulos, P.-Y. Chen, F. Lu, F. Demmerle, G. Boehm, M. C. Amann, A. Alù, and M. A. Belkin, "Giant nonlinear response from plasmonic metasurfaces coupled to intersubband transitions," Nature **511**, 65–69 (2014).
36. J. Mäkitalo, S. Suuriniemi, and M. Kauranen, "Boundary element method for surface nonlinear optics of nanoparticles," Opt. Express **19**, 23386–23399 (2011).
37. J. Butet, B. Gallinet, K. Thyagarajan, and O. J. F. Martin, "Second harmonic generation from periodic arrays of arbitrary shape plasmonic nanostructures: a surface integral approach," J. Opt. Soc. Am. B **30**, 2970–2979 (2013).
38. A. M. Kern and O. J. F. Martin, "Surface integral formulation for 3D simulation of plasmonic and high permittivity nanostructures," J. Opt. Soc. Am. A **26**, 732–740 (2009).
39. P. B. Johnson and R. W. Christy, "Optical constants of the noble metals," Phys. Rev. B **6**, 4370–4379 (1972).
40. F. X. Wang, F. J. Rodriguez, W. M. Albers, R. Ahorinta, J. E. Sipe, and M. Kauranen, "Surface and bulk contributions to the second-order nonlinear optical response of a gold film," Phys. Rev. B **80**, 233402 (2009).
41. G. Bachelier, J. Butet, I. Russier-Antoine, C. Jonin, E. Benichou, and P.-F. Brevet, "Origin of optical second-harmonic generation in spherical gold nanoparticles: local surface and nonlocal bulk contributions," Phys. Rev. B **82**, 235403 (2010).
42. T. F. Heinz, *Second-Order Nonlinear Optical Effects at Surfaces and Interfaces*, H.-E. Ponath and G. I. Stegeman, eds. (Elsevier, 1991).
43. J. I. Dadap, J. Shan, K. B. Eisenthal, and T. F. Heinz, "Second-harmonic Rayleigh scattering from a sphere of centrosymmetric material," Phys. Rev. Lett. **83**, 4045–4048 (1999).
44. J. I. Dadap, J. Shan, and T. F. Heinz, "Theory of optical second-harmonic generation from a sphere of centrosymmetric material: small-particle Limit," J. Opt. Soc. Am. B **21**, 1328–1347 (2004).
45. G. Gonella, W. Gan, B. Xu, and H.-L. Dai, "The effect of composition, morphology, and susceptibility on nonlinear light scattering from metallic and dielectric nanoparticles," J. Phys. Chem. Lett. **3**, 2877–2881 (2012).
46. C. Ciracì, E. Poutrina, M. Scalora, and D. R. Smith, "Origin of second-harmonic generation enhancement in optical split-ring resonators," Phys. Rev. B **85**, 201403(R) (2012).
47. M. W. Klein, M. Wegener, N. Feth, and S. Linden, "Experiments on second- and third-harmonic generation from magnetic metamaterials," Opt. Express **15**, 5238–5247 (2006).
48. J. Nappa, G. Revillod, I. Russier-Antoine, E. Benichou, C. Jonin, and P.-F. Brevet, "Electric dipole origin of the second harmonic generation of small metallic particles," Phys. Rev. B **71**, 165407 (2005).
49. G. Bachelier, I. Russier-Antoine, E. Benichou, C. Jonin, and P.-F. Brevet, "Multipolar second-harmonic generation in noble metal nanoparticles," J. Opt. Soc. Am. B **25**, 955–960 (2008).
50. A. Benedetti, M. Centini, M. Bertolotti, and C. Sibilia, "Second harmonic generation from 3D nanoantennas: on the surface and bulk contributions by far-field pattern analysis," Opt. Express **19**, 26752–26767 (2011).
51. D. de Ceglia, M. A. Vincenti, C. de Angelis, A. Locatelli, J. W. Haus, and M. Scalora, "Role of antenna modes and field enhancement in second harmonic generation from dipole nanoantenna," Opt. Express **23**, 1715–1729 (2015).
52. K. D. Osberg, N. Harris, T. Ozel, J. C. Ku, G. C. Schatz, and C. A. Mirkin, "Systematic study of antibonding modes in gold nanorod dimers and trimers," Nano Lett. **14**, 6949–6954 (2014).